Current Applied Science and Technology Vol. 23 No. 1 (January-February 2023)

Research article

Chemostratigraphy of Two Wells in Niger Delta Basin: An Integrated Approach to Stratigraphic Study

Kiamuke Itiowe[1]*, Frank Adebayo Lucas[2], Charles Ugwu Ugwueze[3] and Osaki Lawson-Jack[4]

[1]*Department of Earth Sciences, Arthur Jarvis University, Akpabuyo, Cross River State, Nigeria*
[2]*Department of Geology, University of Benin, Benin City, Edo State, Nigeria*
[3]*Department of Geology, University of Port Harcourt, Port Harcourt, Rivers State, Nigeria*
[4]*Department of Physical and Chemical Sciences, Elizade University, Ilara Mokin, Ondo State, Nigeria*

Received: 24 October 2021, Revised: 1 May 2022, Accepted: 20 June 2022

DOI: 10.55003/cast.2022.01.23.010

Abstract

Keywords

geochemical characterization;
elemental chemostratigraphy;
geochemical boundaries;
inorganic geochemistry;
Niger Delta Bain

Chemostratigraphic characterization and correlation was carried out on two wells in the Niger Delta with the aim to integrate chemostratigraphic data with already existing biostratigraphic information from the Niger Delta. Shale cutting samples taken within the interval of interest from both wells were subjected to inorganic geochemical and mineralogical analysis using energy dispersive x-ray fluorescence spectrometry (ED-XRF) and x-ray diffractometry, respectively. The key elements used for chemostratigraphic characterization and correlation for both wells were Al_2O_3, K_2O, Na_2O and Fe_2O_3. Four geochemical packages and three geochemical boundaries at depths of 8265ft, 9120ft and 10080ft were identified in #3 well, while two geochemical packages and one geochemical boundary at 4500ft were identified in the Sahaiawei-1 well. The primary mineralogical controls on the elemental variations identified in both wells were clay minerals (kaolinite, illite/muscovite, and chlorite), plagioclase, microcline, jarosite and pyrite. In this study, chemostratigraphic data was integrated with already existing biostratigraphic information, enabling the establishment of some informal geochemical markers in the Northern Delta and Greater Ughelli depobelts. Our research results will improve on the inorganic geochemistry and chronostratigraphic charts of the Niger Delta, and it will in future facilitate seismic interpretation and the identification of the Niger Delta petroleum play elements.

*Corresponding author: E-mail: kiamukeitiowe@yahoo.com

1. Introduction

Chemostratigraphy is a stratigraphic method that involves the use of variations in whole rock inorganic geochemistry to characterize and subdivide sedimentary sequences into geochemically distinct packages and units, and correlation of strata in sedimentary basins [1-4]. Chemostratigraphy as a tool for correlation has been used by different workers around the world. The use of integrated inorganic geochemistry, whole rock x-ray diffraction, and heavy mineral analysis as an example of alternative correlation technique in a low-accommodation setting, non-marine hydrocarbon sequence in Lower Cretaceous Manville Basal Quartz succession was carried out by Ratcliffe *et al*. [5] who stated that it was possible to elucidate the main mineralogical controls on key elements. By understanding the mineralogical controls on sediment geochemistry, it is possible to comment on the geological controls responsible for geochemical differentiation.

Chemostratigraphy has been used as a tool for correlation in the Upper Carboniferous Formation which consists in virtually barren and mainly red-bed sequences that contain important gas reserves. However, well placement and reservoir development have been hampered by a lack of reliable data and stratigraphical frameworks [1]. Chemostratigraphy was employed to produce a detailed high resolution correlation scheme for structures encountered in Devonian, Carboniferous and Permian sediments [6]. Craigie *et al*. [6] aimed to integrate existing biostratigraphic information with his chemostratigraphic study as part of a multidisciplinary approach to correlate the reservoir. In the same work, they stated that establishing a chemostratigraphic zonation follows an interpretative methodology. Craigie *et al*. [7] presented a chapter that was an overview of the analytical techniques used in chemostratigraphy, as well as information on methods that were mainly poorly understood. They highlighted the basis on which element: mineral links are defined, the manner in which key elements and ratios are picked, and on what principle the geochemical boundaries are placed. Craigie [8] wrote a book which provided information on the comprehensive understanding of the applications of chemostratigraphy. The book offers details on sample preparation, methodology, the techniques used to establish the mineralogical affinities of elements, and the diverse principles underlying the building of chemostratigraphic schemes. In the absence of biostratigraphic data and arduousness in using lithostratigraphy for correlation, Craigie [9] chose to employ chemostratigraphy for the Silurian Qusaiba Member, and studied five wells in the Eastern part of Saudi Arabia.

Prundeanu *et al.* [10] used a new technique of chemosteering (or elemental geochemistry analysis) as an option for the identification of Cenomanian, Turonian–Coniacian–Santonian, Campanian and Eocene strata. This enabled the precise positioning of the horizontal development wells within the desired reservoir interval. The use of LWD azimuthal resistivity to steer and land the wellbore within the reservoir and also to monitor distance-to-bed boundary for the cap rock was carried out by Mejia *et al.* [11]. With the reservoir formation possessing low contrast resistivity and low natural resistivity, advanced cuttings analysis enabled steering decisions to be made based on the variation of microscale elemental ratios and abundance. The well was positioned and drilled within the target zone for optimal recovery. Fačevicova *et al*. [12] carried out elemental geochemistry of fourteen D/C boundary sections in six key areas across Europe with the aim of selecting globally correlatable elemental proxies for the D/C boundary. They analyzed geochemical data derived from EDXRF and stated that the concentrations of terrigenous elements (Al, K, Zr, Ti and Rb) were mainly controlled by calcium carbonate in the limestone facies. Hence, their variations can be related to carbonate production in the sea.

Chemostratigraphy as a stratigraphic technique is not older than twenty years. In the Niger Delta, there is no published work on the use of chemostratigraphy for characterization and correlation of wells, and this study will be the first of its kind to use chemostratigraphic techniques for characterization and correlation in the delta. There is need to provide more information on the

inorganic geochemistry of the Niger Delta sediments, as well as to improve on its chronostratigraphic chart. The aim is to integrate chemostratigraphical data with already existing biostratigraphic information for characterization and correlation in the Niger Delta.

The stratigraphic sequence of the Niger Delta consists of coarsening upward sediments that are diachronous [13, 14]. The Cenozoic Niger Delta Stratigraphy is a direct product of the various depositional environments. The earliest information on the geology of the Niger Delta was reported [15-17] and also in subsequent studies [14, 18-21]. Stratigraphically, the delta is divided into three formations, which are the Akata, Agbada and Benin formations [21] (Table 1). The age of these formations decreases basin-ward, reflecting the general regression of depositional environments within the Niger Delta clastic sedimentary wedge.

The study area is located in two depobelts in the Niger Delta, the Northern Delta and Greater Ughelli Depobelts (Figure 1). The two wells are positioned about 36km apart. The two wells are geographically located between latitude 5°30'N and 6°N and longitude 5°30'E and 6°E.

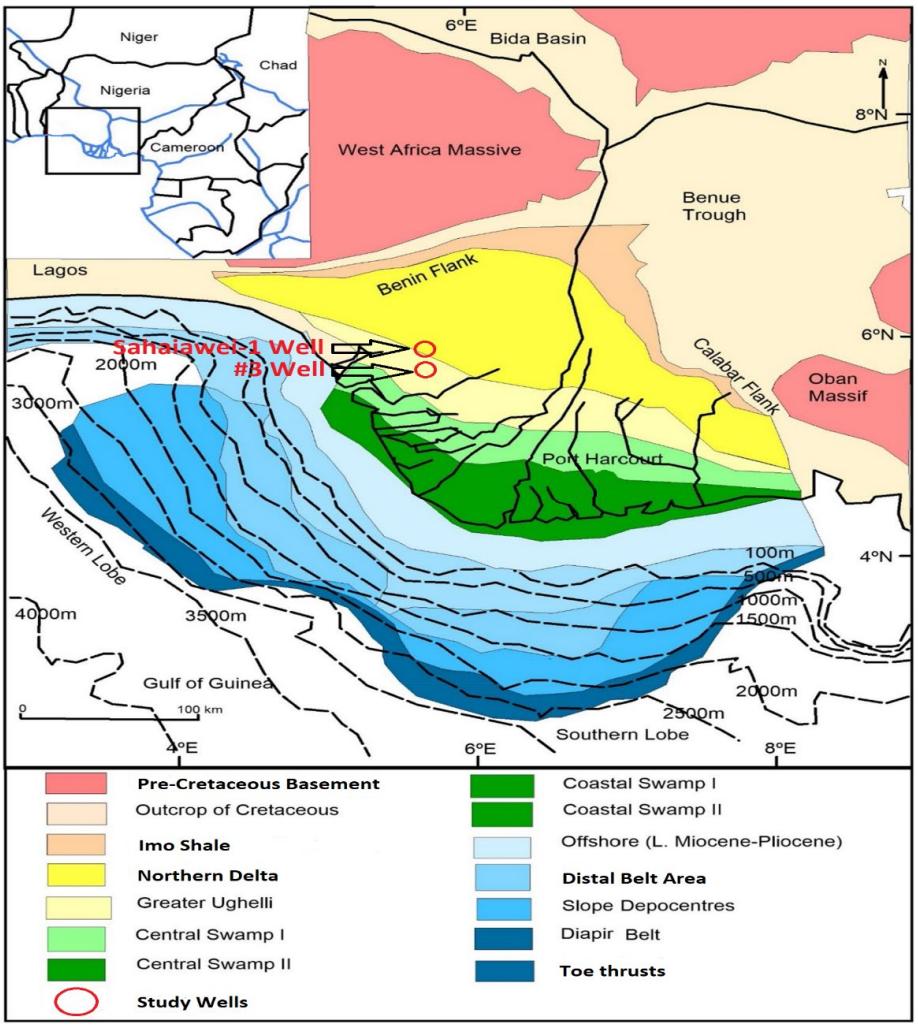

Figure 1. Location map of study well, indicated by red circles [22, 23]

Table 1. Age and formations of the Niger Delta Basin [16]

Subsurface stratigraphy		
Youngest known age	**Formation**	**Oldest known age**
Recent	Benin Formation	Oligocene
	Afam Shale Member	
Recent	Agbada Formation	Eocene
Recent	Akata Formation	Eocene Paleocene Maastrichtian
	Equivalent not known	

A summary of previous work on the biostratigraphy of #3 and Sahaiawei-1 wells: Palynological analysis and foraminifera biostratigraphy were carried out on seventy ditch cutting samples from the shaly and sandy shale lithologies at different intervals between 15ft to 11,430ft in #3 Well. The palynological analysis allowed the recovery of 1312 palynomorphs, which included 1150 miospores. Dinocysts and ancillary microfossils constituted a total of 162 [24]. Some of the index/age marker species that were used for palynological zonation and age determination are*: Acrostichum aureum, Arecipites exilimuratus, Cicatricosisporites dorogensis, Elaeis guineenes, Magnariatites hawardi, Monoporites annulatus, Pachydermites diederixi, Pereglinipollis nigericus, Praedopollis flexibilis, Racemonocolpites hians, Retibrevitricolporites protudensis, Retibrevitricoporites obodoensis, Verrucatosporites usmensis* and *Zonocostites ramonae.* Five palynological zones: the P540, P560, P580, P620-P630 and P650-P670 zones of Evamy *et al*. [14] were identified using the palynological characteristics of the index/age diagnostic markers [24]. On the other hand, the foraminifera biostratigraphy gave a recovery of 26 foraminifera species and 4 foraminifera genera [25]. Calcareous and arenaceous species were mostly recorded, with planktic species generally absent. The calcareous species accounted for about 70% of the total population. Some of the calcareous marker species recorded include: *Florilus costiferum (Nonion 6), Florilus atlanticus, Lenticulina grandis, Hanzawaia concentrica, Valvulineria sp., Altistonia scalaris, Hopkinsina bononiensis, Spirosigmoilina oligocaenica* and *Bolivina dertonensis.* The arenaceous foraminifera species accounted for about 30% of the total population, which was of low diversity. Some of the arenaceous foraminifera species that were used for zonation and age determination were*: Poritextularia panamensis, Eggerella scabra, Reophax* sp.*, Spiroplectammina wrightii, Haplophragmoides* sp.*, Alveolophragmium crissum* and *Haplophragmoides narivaensis*. Two foraminifera zones (Lower N2- N4) and (N4-N5) of Blow [26, 27] were delineated for #3 Well [25].

Furthermore, biostratigraphy was carried out on 50 ditch cutting samples within the shaly and sandy shale lithologies at different intervals between 1800ft to 10680ft in the Sahaiawei-1 well [28]. The palynological study allowed the recovery of 757 palynomorphs which included 689 miospores. Dinocysts and ancillary microfossils accounted for 68. Some of the identified palynomorphs used for palynological biozonation and age determination were: *Auriculopollenities*

echinatus, Bombacacidites sp.*, Bulanopollis minutus, Cinctiporipollis mulleri, Ctenolophomidites costatus, Ctenolophonidites* sp.*, Cyathidites minor, Dualaidites laevigatus , Elaeis guineenses, Erecipites* sp.*, Gemmatriporites* sp.*, Granulatisporites* sp.*, Grimsdalea diversiclavata, Grimsdalea polygonalis, Laevigatosporites haarditii, Leiotriletes* sp.*, Magnastriatites grandiosus, Margocolpites vanwiihei, Monoporites annulatus, Omnipites africanus, Pachydermidites diederixi, Psilamonocolpites marginatus, Psilatricolporites crassus, Psilatricolporites* sp.*, Proxapertites cursus, Proxapertites operculatus, Psilamonocolporites sp., Psilastephanocolporites* sp.*, Psilatricolporites costatus, Retibrevitricolpites triangulatus, Retidiporites magdalenensis, Retimonocolpites obaensis, Retimonocolpites* sp.*, Retitricolpites bendeensis, Retitricolporites irregularis, Retitricolporites* sp.*, Scabratriporites simpliformis, Striatricolporites melane, Spinizonocolpites echinatus, Striamonocolpites rectostriatus, Verrucatosporites usmensis, Verrucatosporites tenellis* and *Zonocostites ramonae*. Four palynological zones: P330-P430, P450, P470 and P480 of Evamy *et al*. [14] were established using the palynological characteristics of the index/age diagnostic markers [28]. On the other hand, the foraminifera study gave a recovery of 2365 forms, with planktic foraminifera consisting of 154 forms, while calcareous and arenaceous foraminifera accounted for 2162 and 49 of the total foraminifera population, respectively [29]. Some of the planktic foraminifera species used for foraminifera biozonation and age determination were: *Globorotalia rohiri, Globigerian ampliapertura, Globorotalia increbescens, Morozovella clavata, Globorotaria pseudomennardii, Globorotalia wilcoxensis, Globigerina triloculiniodes, Globorotalia compressa, Globorotalia mikanna, Acarinina mckannai, Globorotalia ehrenbergi* and *Hedbergella holmdelensis.* Some of the calcareous foraminifera species used for foraminifera biozonation and age determination were: *Heterolepa pseudoungeriana, Florilus costiferum, Ammobaculites strathemensis, Eponides berthlotianus, Eponides eshira, Uvigerina hourquii, Epistominella berthelotianus, Eponides Africana, Valvulineria* sp.*, Altistonia tenuis, Lenticulina pseudomamillegerus, Eponides pseudoelevatus, Valvulineria martinezensis, Hopkinsina bononiensis, Bolivina tennicostata, Anomalinoides madrugaensis, Bolivina afra, Orthokarstenia clavata, Bolivina* sp. and *Bulimina* sp. The arenaceous foraminifera species used for foraminifera biozonation and age determination were: *Haplophragmoides* sp.*, Ammobaculites* sp.*, Bathysiphon* sp.*, Ammobaculites coprolithiformis* and *Textularia* sp. Five foraminifera zones: the M18, P1-P2, P3-P4, P5-P6/P7 and P7-P13 zones of Blow [26, 27] were established [29].

Finally, based on the sequence stratigraphic study that was carried out in the areas, two sequence boundaries and one maximum flooding surface were identified in #3 well [30] (Figure 2), while one sequence boundary and three maximum flooding surfaces were identified in Sahaiawei-1 well [30] (Figure 3).

2. Materials and Methods

Twenty-eight ditch cutting samples from #3 well within the depth range of 6255ft to 11205ft and 20 ditch cutting samples from Sahaiawei-1 well within the depth range of 1680ft to 10620ft were selected for XRF spectrometry. These samples were picked from the shaly intervals of interest and were constrained to the palynological zones of both wells. The samples were processed to determine the major oxide, trace and rare earth elements using standard XRF preparation technique. XRF provided information on the whole rock inorganic geochemistry that was used for chemostratigraphic characterization and correlation. The ditch cutting samples were assessed for 48 elemental constituents (11 major oxides and 37 trace/REE) using x-ray fluorescence analytical method at Nigeria Geological Survey Agency, Kaduna. The major elements were used for the characterization and correlation because they show subtle variation and stratigraphic control across the two wells. The trace and rare earth elements did not exhibit stratigraphic control across the wells.

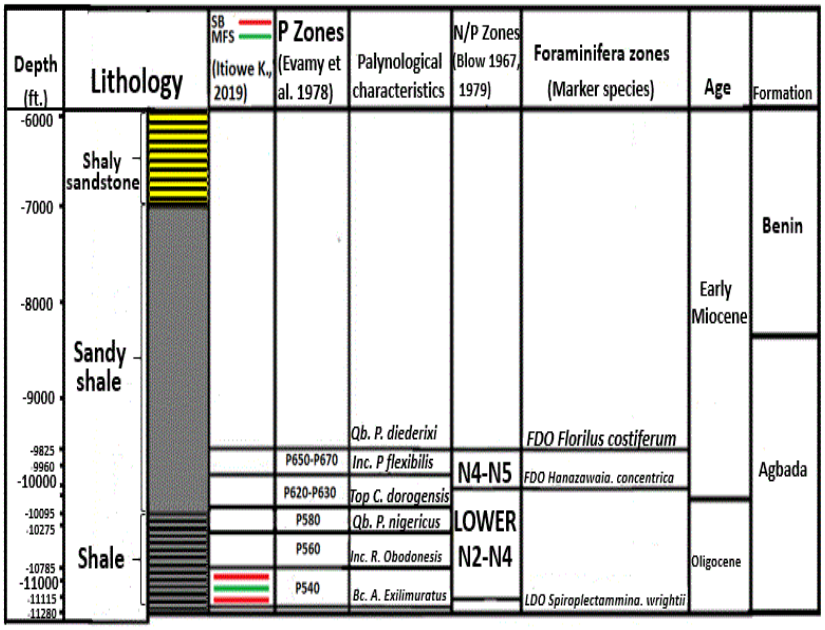

Figure 2. Showing the summary of the sequence stratigraphic elements for #3 well (modified from Itiowe [30])

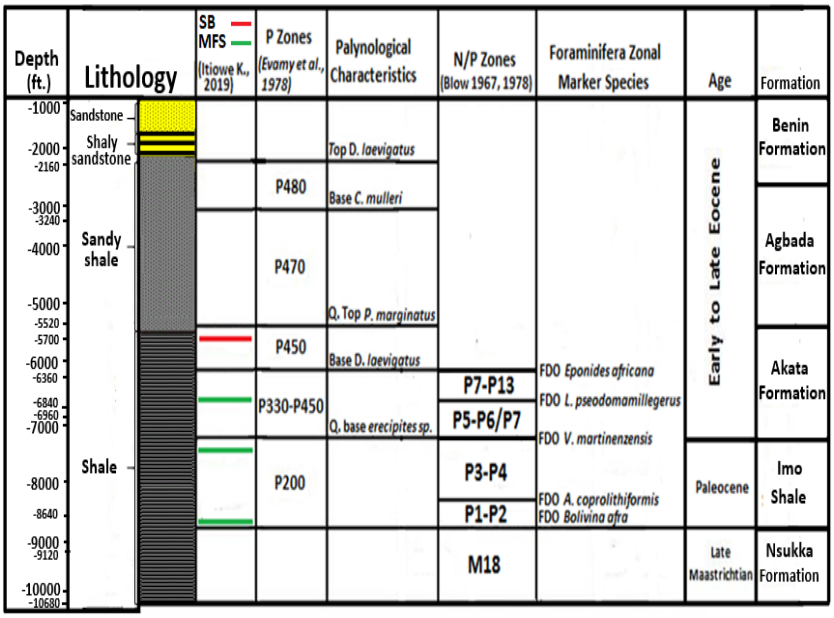

Figure 3. Showing the summary of the sequence stratigraphic elements for Sahaiawei-1 well (modified from Itiowe [30])

XRF is an analytical technique which is nondestructive. It measures the elemental constituents of minerals. The XRF spectrometer analyzes the chemical composition of a sample by measuring the emitted fluorescence x-rays from the sample when a primary source excites it. A group of characteristics fluorescent x-rays that is peculiar to a specific element in the sample is produced by each element in a sample. For more information on history and use of XRF analyzer, refer to the work of Lemiere [31]. Hence, x-ray spectroscopy is good for both qualitative and quantitative analysis of the composition of a material. The sample preparation and analysis take less than 20 min. Five grams of each shale cutting sample was oven dried for 4 h at 80ºC in order to remove the moisture. The sample was milled using a planetary micro mill pulverisette (Arget pulverizing machine). In order to ensure homogeneity of the sample, the pulverized sample was allowed to passed through 75 micro mesh sieves. Each powdered sample was packed and labeled into a sample cup and placed into an Energy Dispersive X-Ray fluorescence (EDXRF) spectrometer of model "Minipal 4" for the analysis. The following standards were set on the machine: elemental composition to be determined, the nature of sample to be analyzed was set as loose powder, the detection limit for the major oxides including Al_2O, K_2O, Na_2O and Fe_2O_3 was < 0.1 %, while the detection limit for the trace and rare earth elements was < 5 ppm. Kapton was the selected filter for the major oxides and Al-thin for the trace and rare earth elements, 25 kilovolts for major oxides, trace elements/rare earth metals, and 100 s was the measurement time for each sample. For further inquiry about the sample preparation and how XRF analysis works, refer to Craigie [8].

On the other hand, a total of 16 samples were subjected to x-ray diffraction analysis. Eight samples from each of the wells were selected from the samples that had been taken for XRF spectrometry. The samples were processed using standard XRD preparation technique. XRD analysis is a technique that is used for analyzing the crystallographic structure of a material. It works effectively on crystalline materials. The XRD principles obey Bragg's law, which states that the x-rays reflected from dissimilar crystal layers with lengthy range order go through constructive interference [32]. It works by exposing a material to incident x-ray radiation and then estimating the scattering angles and intensities of the x-rays that leave the material. For more information on principles of XRD diffractometry, refer to the work of David *et al*. [32]. The sample preparation takes less than 18 h. Each shale cutting sample (3 g) was weighed and freeze-dried for about 12 h before milling. The sample was pulverized for about 10 min, and methanol was used as the grinding agent. In order to ensure good mixing, the dried samples were passed through 250 micro sieves. About 0.5 g of the sample was placed on a sample holder ring and preparation was done using the back loading technique. The prepared powdered sample was placed into the diffractometer (Panalytical Aeris Diffractometer) for analysis. The diffractometer had a pixel detector fixed with Fe filtered Co-Kα radiation for analysis. X-pert highscore plus software was used to identify the phases during the analysis. The Rietveld method was used to estimate the relative amount (weight %). For further inquiry on sample preparation and how XRD analysis works, refer to Will [33] and Moore and Reynolds [34]. The XRD provided the information on the mineralogy in which the likely minerals control the distribution of the key elements that were crucial in the chemostratigraphic characterization and correlation.

In studies dealing with chemostratigraphic correlation, different correlation schemes were prepared for the sandstone and shale samples [9, 35]. In this study, shale represented the lithological component. The main purpose of this study was to divide the formations in #3 and Sahaiawei-1 into distinct geochemical packages. The elements that showed subtle variation and stratigraphic control across the wells were used for the chemostratigraphic characterization and correlation. For these purposes, the use of all available elements is crucial and essential. However, the EDXRF resolution is not sufficient for detection of a high range of trace elements, including some elements concentrated in heavy minerals. Therefore, the major oxides were used for characterization and correlation in this study. After careful scrutiny, a few numbers of "key" elements were selected for chemostratigraphic purposes. The geochemical packages and boundaries assessment used the

percentage of selected ratios that fell under specifically chosen cut offs. Plots of the data of key elements against depth in the form of profiles were used to check for useful proxies and determine the geochemical packages and boundaries. Thereafter, the construction of binary diagrams was carried out to buttress where the chemostratigraphic boundaries were placed. Finally, the determination of the likely mineralogical controls on key elements that were used for the chemostratigraphic characterization and correlation was carried out. The mineralogical control on key elements can be achieved through whole rock x-ray diffractometry, petrographic analysis, or principal component analysis. But in this study, the mineralogical control of the key elements was determined by x-ray diffraction.

3. Results and Discussion

3.1 Geochemical packages

The geochemical packages were characterized based on key elements that showed subtle variation and stratigraphic control across both wells. The key elements were K_2O, Na_2O, Fe_2O_3 and Al_2O_3 which were consistent in both wells. The #3 well has four geochemical packages and three geochemical boundaries (Figure 4). From the plot of K_2O, there was a general increase in trend from 8265ft (base of package 4) to 11205ft (base of package 1); above this point, the K_2O values fluctuated between 0.9% to 1.8% (Table 2). The plot of Na_2O shows a general increase in trend from 8265ft (base of package 4) to 11205ft (base of package 1). Above this point, there was an increase in the Na_2O trend (Figure 4). For the Fe_2O_3 plot, there was a general increase in trend from 8265ft (base of package 4) to 11205ft (base of package 1); above this point the Fe_2O_3 trend remained lower (Figure 4).

On the other hand, the Sahaiawei-1 well had two geochemical packages and one geochemical boundary (Figure 4). From the plot of K_2O and Na_2O, there was a general increase from 10620ft (base of package 1) to 7440ft (about the middle of package 1) and then values trended downward to 4500ft. Above the geochemical boundary at 4500ft, the trends of K_2O and Na_2O decrease were generally low. For Fe_2O_3, there was a general increase in trend from the base of package 1 (at 10620ft) to the geochemical boundary at 4500ft, the trend decreased to 3%, then showed further increase. The geochemical packages and geochemical boundaries for #3 well and Sahaiawei-1 well have been differentiated in the binary diagrams (Figures 5a, 5b and 5c) and (Figures 5d, 5e and 5f), respectively.

3.1.1 Package 1

This package in #3 well was characterized by higher trends with K_2O values (1.24% to 3.10%) and Na_2O values (0.11% to 1.11%) as compared to lower trends in packages 2 to 4 (Figure 4); the average of K_2O and Na_2O values in package 1 were 2.241% and 0.515%, respectively (Table 2). In Sahaiawei-1 well, package 1 had higher trends of K_2O values (0.98% to 2.77%) and Na_2O values (0.44% to 0.98%) as compared to lower trends of K_2O and Na_2O in package 3, and the averages of K_2O and Na_2O values in package 1 were 1.9% and 0.6%, respectively (Table 3). Package 1 in #3 well was comparable to package 1 in Sahaiawei-1 well based on the higher K_2O and Na_2O values (Figure 4).

3.1.2 Package 2

This package was only seen in #3 well. The package had higher K_2O values (1.05% to 2.40%) and lower Na_2O values (0.05% to 0.40%). The averages of K_2O and Na_2O values in package 2 were 2.122% and 0.243%, respectively. This package was not seen in Sahaiawei-1 well, which could have been a result of low resolution zone or sampling gap.

3.1.3 Package 3

Package 3 in #3 well was characterized by lower K_2O values (0.78% to 1.87%) and Na_2O values (0.18% to 0.58%) as compared to higher K_2O and Na_2O values in package 1. The average K_2O and Na_2O values in this package were 1.276% and 0.235%, respectively. This package was also characterized by a decreasing Fe_2O_3 trend from the graphical plot (Figure 4). Package 3 was seen in Sahaiawei-1 well based on the lower K_2O and Na_2O trends as compared to the higher K_2O and Na_2O trends in package 1. This package 3 in #3 well could be correlated to package 3 in Sahaiawei-1 based on the lower K_2O and lower Na_2O values (decreasing trends).

3.1.4 Package 4

This package showed increasing Na_2O trends and lower Fe_2O_3 values (0.98% to 1.80%). The average Na_2O and Fe_2O_3 values in this package were 0.373% and 3.98%, respectively. This package was not seen in Sahaiawei-1 well which could have been a result of sampling gaps.

3.2 Geochemical boundaries

3.2.1 Geochemical boundary 1 (10080ft and 4500ft)

The geochemical boundary 1 for #3 well was placed at 10080ft (Figure 4). At that depth, there appeared to be a point from bottom upwards where the K_2O values decreased abruptly from 3.10% to 2.01% and Na_2O values increased from 0.24% to 0.34% (Table 2). Within package 1 to package 2 at 10080ft boundary, there was a decrease from bottom to top of the average K_2O and Na_2O values from 2.241% and 0.515% below the boundary to 2.122% and 0.243% above the boundary, respectively (Table 2). Geochemical boundary 1 can be discerned from the binary diagrams by the separation of the clustering of the package 1 (olive green diamonds) and clustering of package 3 (blue triangles) (Figures 5a, 5b and 5c). The geochemical boundary 1 in Sahaiawei-1 well enabled the well to be divided into two geochemical packages (Figure 4). The boundary was placed at 4500ft because at this depth, there was a decrease in K_2O values from 1.5% to 1.0%, an increase in the value of Na_2O from 0.031% to 0.5% and increase in Fe_2O_3 value from 4.79% to 6.81% (Table 3). Below 4500ft boundary, the average K_2O dropped from 1.9% to 0.9% above the boundary, and the average Na_2O dropped from 0.6% below the boundary to 0.18% above the boundary, and the average Fe_2O_3 value increased from 5.73% below the boundary to 6.02% above the boundary. Therefore, at this point of 4500ft, the geochemical boundary was placed. Below the geochemical boundary value at 4500ft, there were higher K_2O and Na_2O values and above the boundary the K_2O and Na_2O values were generally lower. This geochemical boundary is bolstered by a blue line which separates package 1 (clustering of olive green diamonds) from package 3 (blue triangles) in the binary diagrams (see Figures 5d, 5e and 5f).

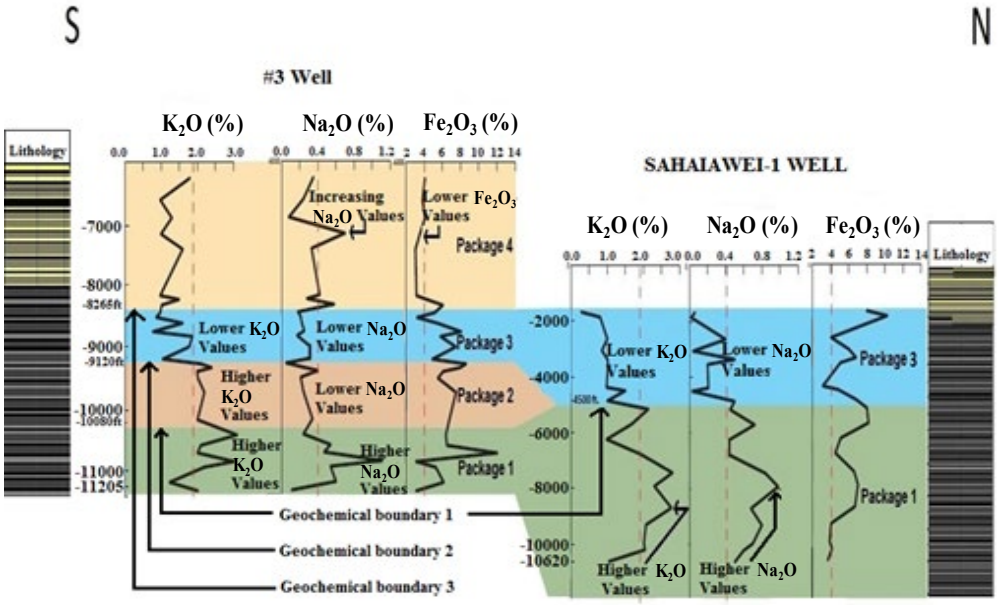

Figure 4. Chemostratigraphic characterization and correlation across both wells

3.2.2 Geochemical boundary 2 (9120ft)

The geochemical boundary 2 for #3 well was placed at 9120ft. At this depth, from bottom to top, there was a decrease in K_2O value from 2.10% to 1.05%, an increase in Na_2O value from 0.05% to 0.31% and a decrease in Fe_2O_3 value from 8.60% to 4.89% (Table 2). At 9120ft boundary in #3 well, the average K_2O, Na_2O and Fe_2O_3 values decreased from bottom to top from 2.122%, 0.243% and 7.06% to 1.275%, 0.235% and 5.71%, respectively, and at this depth geochemical boundary 2 was placed (Figure 4).

3.2.3 Geochemical boundary 3 (8265ft)

The geochemical boundary 3 was placed at 8265ft (Figure 4). At this depth, there was an increase in Na_2O and Fe_2O_3 values from bottom to top from 0.18% to 0.58% and 5.14% to 6.05%, respectively (Table 2). Below the 8265ft boundary, the average Na_2O increased from 0.235% below the boundary to 0.3725% above the boundary and Fe_2O_3 decreased from 5.71% below the boundary to 3.98% above the boundary, so at this depth below 8265ft the geochemical boundary 3 was placed (Figure 4). This geochemical boundary 3 can be discerned from the binary diagrams by the separation of the clustering of package 3 (blue triangles) and package 4 (orange circles) (Figures 5a, 5b and 5c).

3.3 Mineralogical control on key elements

A correlation for both wells was achieved based on inorganic geochemistry; this correlation was independent on the geology and mineralogy (Figure 4). Therefore, there was need to understand the likely mineralogical control on these geochemical key elements that were used for the

Table 2. Major oxides of #3 Well for chemostratigraphic characterization

Depth (ft.)	Oxide composition (%)											
	SiO_2	MgO	CaO	K_2O	Na_2O	MnO	P_2O_5	Fe_2O_3	TiO_2	Al_2O_3	BaO	LOI
6255	47.33	0.78	3.16	1.80	0.35	0.10	0.003	4.07	1.74	18.40	0.71	15.67
6600	50.00	0.21	1.03	0.98	0.24	0.055	0.002	3.78	0.77	18.60	0.51	20.45
6885	42.90	0.22	1.80	1.30	0.08	0.044	nd	4.06	1.69	20.32	0.90	18.40
7140	70.30	0.05	0.95	1.00	0.70	0.031	0.002	3.50	1.99	10.02	0.29	6.10
7380	81.80	0.08	0.98	1.60	0.33	0.02	nd	3.01	1.60	8.25	0.34	1.20
8115	42.06	0.45	2.16	0.98	0.42	0.038	0.0006	3.13	1.56	20.12	1.80	15.01
8175	50.50	0.50	1.03	1.50	0.28	0.037	nd	4.28	1.48	19.42	0.38	17.30
8265	60.90	0.74	2.30	1.02	0.58	0.029	0.0009	6.05	2.38	11.04	0.94	8.05
8385	42.50	0.09	1.40	0.98	0.18	0.042	0.003	5.14	2.16	20.94	0.53	18.05
8460	84.20	0.009	0.71	0.87	0.21	0.010	nd	3.20	1.44	4.40	0.41	1.01
8550	44.50	0.12	1.52	1.60	0.22	0.045	0.002	5.44	2.00	20.08	0.64	17.40
8685	38.90	0.31	1.58	0.78	0.25	0.049	0.0008	8.07	1.67	19.30	0.74	17.80
8760	42.10	0.40	2.37	1.87	0.17	0.042	nd	5.77	2.78	19.63	0.49	14.06
8925	38.80	0.32	2.54	1.78	0.31	0.053	0.001	7.48	2.80	21.06	1.00	16.93

Table 2. Major oxides of #3 Well for chemostratigraphic characterization (continued)

Depth (ft.)	Oxide composition (%)											
	SiO_2	MgO	CaO	K_2O	Na_2O	MnO	P_2O_5	Fe_2O_3	TiO_2	Al_2O_3	BaO	LOI
9120	45.20	0.07	1.70	1.05	0.31	0.041	0.0004	4.89	2.08	18.08	0.80	17.24
9195	40.00	0.04	1.10	2.10	0.05	0.039	nd	8.60	2.54	19.05	0.87	15.50
9255	43.08	0.12	1.53	2.40	0.22	0.069	nd	7.93	2.90	18.40	0.67	16.93
9315	42.00	0.06	2.50	2.00	0.40	0.043	nd	6.07	2.68	18.20	1.40	14.01
9420	40.20	0.41	3.26	2.02	0.21	0.056	0.002	5.50	2.35	16.00	0.84	14.68
9645	40.24	0.09	3.98	2.20	0.24	0.077	0.0004	7.50	2.22	19.00	0.43	15.20
10080	42.20	0.35	3.01	2.01	0.34	0.032	0.0010	6.76	2.44	18.00	1.78	15.43
10320	40.60	0.24	8.90	3.10	0.24	0.075	nd	6.38	1.06	16.30	0.75	14.08
10485	40.50	0.44	3.87	2.10	0.54	0.03	nd	6.50	4.19	19.02	0.95	15.03
10605	40.70	0.98	1.22	2.01	0.47	0.060	0.0007	12.04	1.81	18.00	0.55	12.45
10740	43.00	0.12	4.03	3.02	1.11	0.009	0.001	3.09	1.37	17.03	0.90	20.00
10830	43.70	0.30	3.05	2.20	0.54	0.023	0.0005	5.26	2.11	20.07	0.61	16.93
11070	44.00	0.22	2.01	1.24	0.60	0.041	nd	6.14	1.99	18.40	0.62	21.02
11205	45.00	0.12	2.03	2.02	0.11	0.009	0.001	3.09	1.37	20.03	0.90	18.00

LOI = Loss on ignition; nd = not detected

Table 3. Major oxides of Sahaiawei-1 Well for chemostratigraphic characterization

Depth (ft.)	Oxide composition (%)											
	SiO_2	Mgo	CaO	K_2O	Na_2O	MnO	P_2O_5	Fe_2O_3	TiO_2	Al_2O_3	BaO	LOI
1680	42.00	0.04	0.19	0.28	0.06	0.21	0.003	8.01	0.65	17.90	0.07	14.20
1860	45.00	0.002	0.35	0.80	0.02	0.24	0.002	10.26	1.29	14.34	0.10	16.00
2640	47.80	0.87	2.11	1.00	0.40	0.02	nd	4.06	0.77	20.02	0.08	18.04
3060	46.90	0.74	1.87	0.85	0.04	0.025	0.007	6.03	1.40	20.00	nd	18.04
3360	49.40	0.05	2.10	1.00	0.50	0.01	nd	6.81	1.91	17.60	0.10	16.80
3540	45.91	0.30	2.21	1.02	0.20	0.04	nd	5.11	1.70	17.20	0.17	14.60
4380	69.00	0.010	0.53	0.98	0.21	0.079	0.001	3.15	1.03	14.90	0.14	4.08
4500	40.40	0.015	0.827	1.50	0.031	0.038	nd	4.79	1.55	18.08	0.23	18.42
4860	43.10	0.05	2.10	1.00	0.50	0.01	nd	6.81	1.91	17.61	0.10	16.80
5160	41.20	0.45	1.54	2.13	0.45	0.02	0.002	8.02	3.00	18.50	0.20	16.98
5700	38.40	nd	nd	1.67	0.72	0.01	nd	8.20	1.97	21.00	0.33	17.60
6240	39.90	0.12	18.90	0.98	0.44	nd	0.002	5.13	1.21	9.60	1.00	15.00
6780	40.11	0.68	6.70	1.93	0.44	0.07	nd	4..53	1.70	19.20	1.20	15.02
7440	40.85	1.05	nd	2.80	0.84	0.57	0.001	6.60	1.96	15.10	1.80	14.20

Table 3. Major oxides of Sahaiawei-1 Well for chemostratigraphic characterization (continued)

Depth (ft.)	Oxide composition (%)											
	SiO_2	Mgo	CaO	K_2O	Na_2O	MnO	P_2O_5	Fe_2O_3	TiO_2	Al_2O_3	BaO	LOI
7920	40.60	nd	nd	2.30	0.98	0.054	0.002	7.03	2.70	15.00	0.99	14.60
8700	40.80	1.01	6.41	2.77	0.68	0.093	nd	6.70	2.67	16.02	1.10	15.78
9300	34.80	0.23	2.69	2.07	0.80	nd	0.001	4.07	0.60	17.00	18.60	9.40
9960	33.80	1.02	6.65	2.01	0.70	nd	0.003	3.9	0.85	13.00	18.20	7.80
10200	36.40	0.88	8.0	2.04	0.60	nd	nd	4.17	1.10	13.00	12.50	11.06
10620	18.10	0.54	25.00	1.04	0.50	0.067	nd	3.71	0.75	6.12	15.10	16.71

LOl = Loss on ignition; nd = not detected

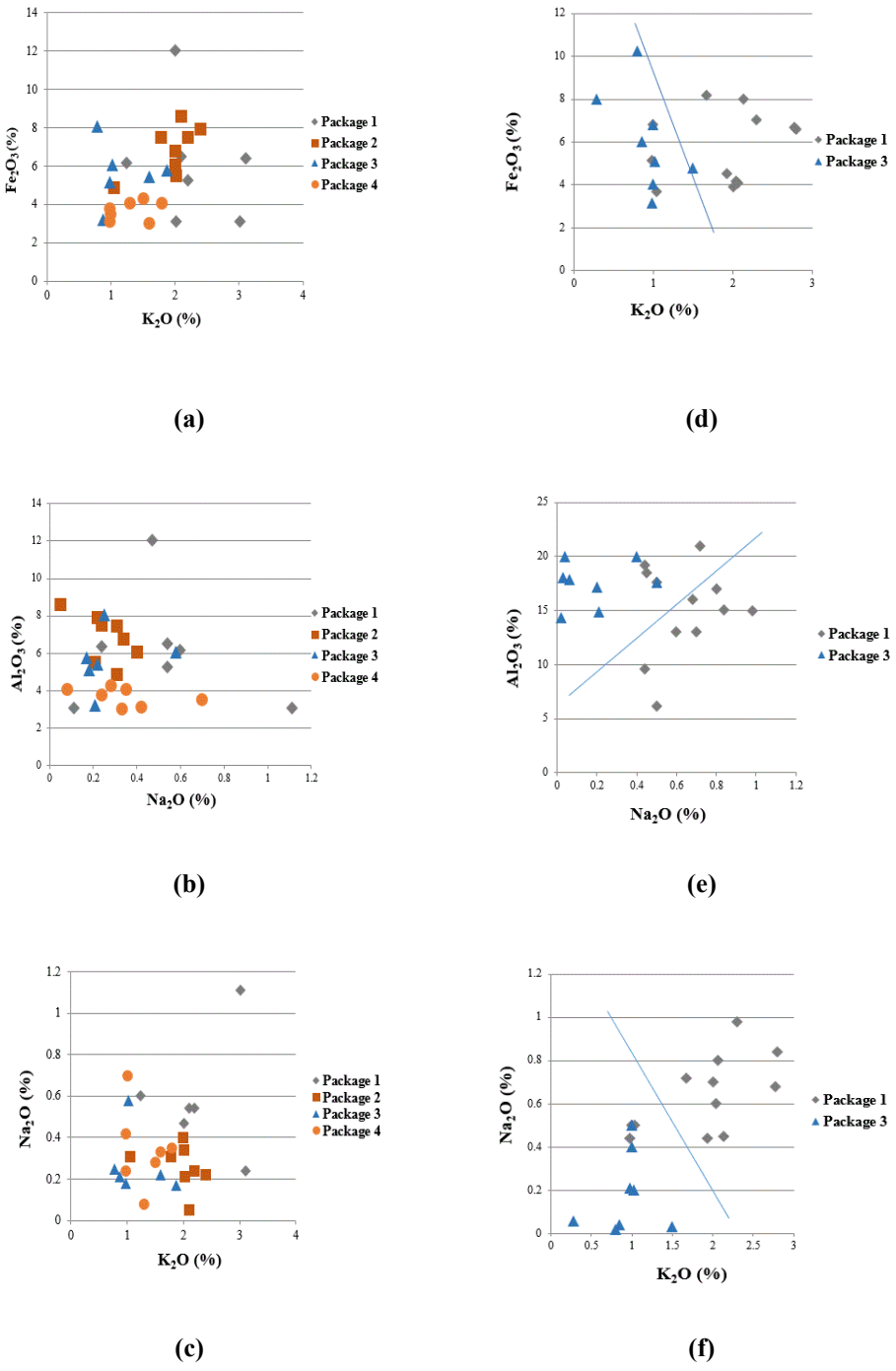

Figure 5. Geochemical differentiation for the Packages in #3 well using K_2O vs. Fe_2O_3 (a); #3 Well using Na_2O vs. Al_2O_3 (b); #3 Well using K_2O vs. Na_2O (c); Sahaiawei-1 well using K_2O vs. Fe_2O_3 (d); Sahaiawei-1 well using Na_2O vs. Al_2O_3 (e); and Sahaiawei-1 well using K_2O vs. Na_2O (f)

correlation. By this, additional geological information was derived from the correlation that was based on inorganic geochemistry. Furthermore, by knowing the minerals that control the key elements, it was be easier to comment on the mineralogical controls that were responsible for the differentiation of the geochemical key elements; hence, it helped in the understanding of the stratigraphic layers.

3.3.1 Mineralogical control on key elements in #3 well

Table 4 shows the bulk mineralogy of #3 well. From the study, some of the key elements within a package were controlled by more than one mineral. For example, in Table 5, Al_2O_3 in #3 well was controlled by more than one mineral, but the major mineral in #3 well that exerted more control on the different packages was kaolinite. The binary diagram of kaolinite against Al_2O_3 below shows a weak linear relationship with a correlation coefficient (R^2) of 0.0204 (Figure 6a). This means that more Al_2O_3 rich minerals could also have been responsible for the distribution of Al_2O_3 in #3 well. K_2O in #3 well was controlled by more than one mineral. For example, in Table 5, microcline, illite/muscovite and jarosite were responsible for the distribution of K_2O in #3 well, but microcline exerted more control than other K_2O containing minerals. The binary diagram of microcline against K_2O (Figure 6b) showed a weak uphill linear relationship with correlation coefficient (R^2) of 0.1011 which meant that there were more K_2O rich minerals that were exerting some control in the distribution of K_2O. It is apparent that plagioclase was responsible for the distribution of Na_2O. From the XRD analysis (Table 4), plagioclase was the only Na_2O containing mineral could be responsible for the distribution of Na_2O in #3 well. The binary plot of plagioclase against Na_2O showed a weak linear relationship with correlation coefficient (R^2) of 0.259 (Figure 6c). This weak uphill trend could be due to more elements in the plagioclase, such as Al_2O_3 and SiO_2, exerted more control on plagioclase than Na_2O. Pyrite and jarosite were the minerals that showed a strong control of Fe_2O_3 in the well (Table 5). Pyrite and jarosite were the minerals that controlled the distribution of Fe_2O_3, whereas illite/muscovite and chlorite made little contribution. The binary diagram plot of pyrite against Fe_2O_3 showed a weak downhill linear relationship with correlation coefficient (R^2) of 0.0261 (Figure 6d). This weak trend may have been because more minerals including illite/muscovite and chlorite exerted some control on the distribution of Fe_2O_3.

3.3.2 Package 1 (10320ft - 11205ft)

For the key element Al_2O_3, the mineral that controlled the distribution of Al_2O_3 within this interval was mainly kaolinite, with little contribution from microcline, plagioclase, and illite/muscovite (Table 5). Kaolinite had higher percentages which were 16.36%, 31.28%, and 14.88% compared to other minerals (microcline, illite/muscovite, chlorite) that contained Al_2O_3 at low or no percentage (Table 4). For the key element K_2O, the mineral that controlled its distribution within this interval was microcline. There was a high concentration of microcline in this interval ranging from 5.32%, 8.05% and 8.11% compared to other minerals (illite/muscovite, jarosite) that contained K_2O (Table 4). The mineral that controlled the distribution of Na_2O was plagioclase. The amounts of plagioclase were 0.74%, 3.29% and 3.65% (Table 4). Fe_2O_3 was controlled by illite/muscovite, with values of 0.72%, 1.42% and 0.78% and pyrite 0.98% and 0.41% (Table 4), but with little contribution from either jarosite and/or chlorite.

3.3.3 Package 2 (9195ft - 10080ft)

For the key element Al_2O_3, the minerals that controlled its distribution were mainly kaolinite with values of 9.69% and 13.6% and microcline with values of 3.34% and 1.57% (Table 5). There was also little contribution from illite/muscovite with values of 0.28% and 0.55% and chlorite with values of 0.28% and 0.08% (Table 4). K_2O was controlled mainly by microcline

Table 4. Bulk XRD percentage for #3 well

Depth (ft)	Clay minerals (%)				Carbonates (%)		Other minerals (%)									Total (%)
	Kao.	Ill./ Mus.	Chl.	Sep.	Car.	Dol.	Qtz.	Pyr.	Ana.	Gyp.	Pla.	Mic.	Jar.	Bar.	Flu.	
6600 (Pk. 4)	0.1	0	0	0.25	0	0	98.6	0.06	0	0.76	0	0	0.23	0	0	100
7380 (Pk. 4)	4.1	0	0	0.3	0	0.2	94.6	0	0	0.61	0	0.19	0	0	0	100
8685 (Pk. 3)	4.78	0.04	0	0.46	0.69	0	91.7	0	0	1.18	0	0	1.14	0	0	99.99
9315 (Pk. 2)	13.6	0.55	0.08	0.66	0.2	0	80.7	0.05	0.04	1.53	0	1.57	0.87	0	0	99.85
9645 (Pk. 2)	9.69	0.28	0.28	0.57	0.07	7.20	76.2	0.63	0	1.67	0	3.34	0	0	0	99.93
10320 (Pk. 1)	14.8	0.78	0.34	0.32	6.60	1.6	61.4	0.41	0.2	1.69	3.65	8.11	0	0	0	99.90
10740 (Pk. 1)	31.28	1.41	0.22	1.57	0.87	0	46.5	0.98	0.47	5.35	3.29	8.05	0	0	0	99.99
11070 (Pk. 1)	16.3	0.72	0	0.92	2.12	0	67.1	0	0.16	3.69	0.74	5.32	2.63	0	0	99.70

Table 5. The mineralogical controls on key elements in #3 well

Packages	Key elements			
	Al_2O_3	K_2O	Na_2O	Fe_2O_3
Package 4 (6255ft-8265ft)	Kaolinite	Microcline, Jarosite	Plagioclase?	Jarosite, Pyrite
Package 3 (8385ft-9120ft)	Kaolinite	Jarosite Illite/muscovite	Plagioclase?	Jarosite, Illite/muscovite
Package 2 (9195ft-10080ft)	Kaolinite, Microcline, Illite/muscovite Chlorite	Microcline, Illite? Jarosite	Plagioclase?	Illite/muscovite, Pyrite, Jarosite Chlorite
Package 1 (10320ft-11205ft)	Kaolinite, Microcline, Illite/muscovite, Chlorite	Microcline, Illite/muscovite, Jarosite	Plagioclase	Illite/muscovite, Pyrite, Jarosite, Chlorite

with values of 3.34% and 1.57%, but with little contribution from either illite/muscovite and/or jarosite. For Na_2O element, the mineral that controlled its distribution was mainly plagioclase. From the XRD analysis, the only Na_2O bearing mineral in #3 well was plagioclase. Fe_2O_3 was mainly controlled by illite/muscovite with values of 0.28% and 0.55% and pyrite with values of 0.63% and 0.05%, but with little contribution from either jarosite and/or chlorite.

3.3.4 Package 3 (8385ft - 9120ft)

The key element Al_2O_3 is primarily controlled by kaolinite with values of 4.78%. K_2O is mainly control by jarosite with value of 1.14% and /or illite/muscovite. Na_2O was controlled by Na containing minerals which may have included plagioclase. Fe_2O_3 was mainly controlled by jarosite with value of 1.14% and/or illite/muscovite with value of 0.04%.

3.3.5 Package 4 (6255ft - 8265ft)

Al_2O_3 was primarily controlled by kaolinite with values of 4.1% and 0.1%. K_2O was primarily controlled by either microcline and/or jarosite. Na_2O was controlled by Na containing minerals that may have included plagioclase, and Fe_2O_3 was primarily controlled by jarosite and/or pyrite.

3.3.6 Mineralogical control on key elements in Sahaiawei-1 well

Table 6 shows the bulk mineralogy of Sahaiawei-1 well. Some of the key elements within a package were controlled by more than one mineral. For example, in Table 7, Al_2O_3 in the Sahaiawei-1 well was controlled by more than one mineral, but the major mineral in Sahaiawei-1 well that exerted more control on the different packages was kaolinite. The binary diagram of kaolinite against Al_2O_3 (Figure 7a), showed a weak uphill linear relationship with correlation coefficient (R^2) of 0.0238, which meant that more Al_2O_3 rich minerals could also have been responsible for the distribution of Al_2O_3 in Sahaiawei-1 well. K_2O in Sahaiawei-1 well was controlled by more than one mineral. Illite/muscovite, jarosite and microcline were responsible

for the distribution of K_2O in Sahaiawei-1 well (Table 7). The binary diagram of illite against

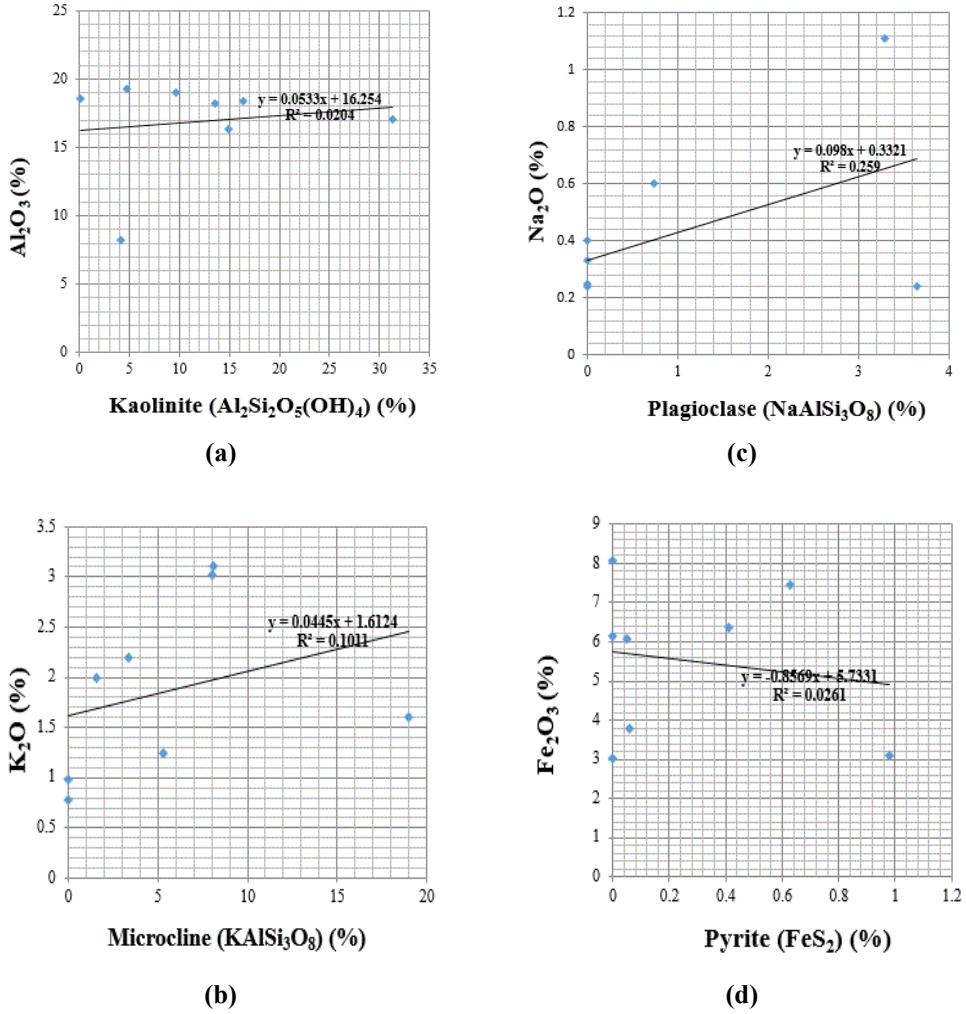

Figure 6. Binary diagram of kaolinite against Al_2O_3 for #3 well (a); microcline against K_2O for #3 well (b); plagioclase against Na_2O for #3 well (c) and pyrite against Fe_2O_3 for #3 well (d)

K_2O (Figure 7b) showed a moderate uphill positive relationship with correlation coefficient (R^2) of 0.4195, which could have meant that some K_2O rich minerals were responsible for the distribution of K_2O in Sahaiawei-1 well. For Na_2O in Sahaiawei-1 well, it was apparent that plagioclase was responsible for the distribution of Na_2O. From the XRD analysis, plagioclase was the only Na_2O containing mineral (Table 6). The binary plot of plagioclase against Na_2O showed a weak linear relationship with correlation coefficient (R^2) of 0.0191 (Figure 7c). This weak trend could have been because more elements in the plagioclase such as Al_2O_3 and SiO_2 were being controlled by the plagioclase rather than Na_2O. Illite/muscovite, chlorite, pyrite and jarosite were the minerals that showed strong control on Fe_2O_3 in the well (Table 7). Illite/muscovite, chlorite and pyrite were the minerals that controlled the distribution of Fe_2O_3 with little contribution from jarosite. The binary diagram plot of pyrite against Fe_2O_3 showed a a weak downhill linear relationship with correlation coefficient (R^2) of 0.0604 (Figure 7d). This weak trend may indicate that more minerals such as illite/muscovite, chlorite and jarosite were exerting some control on the distribution of Fe_2O_3.

3.3.7 Package 1 (4860ft - 10620ft)

For the key element Al_2O_3, the mineral that controlled its distribution within this interval was mainly kaolinite, with little contribution from microcline, plagioclase, illite/muscovite and chlorite (Table 7). Kaolinite had percentage of 7.22%, 37.83%, 29.2%, 25.34%, 23.7% and 39.8% compared to other Al_2O_3 containing minerals with low percentages (Table 6). K_2O was primarily controlled by illite/muscovite with little contribution from microcline. Na_2O was primarily controlled by plagioclase. Fe_2O_3 was primarily controlled by illite/muscovite and/or chlorite and/or pyrite.

3.3.8 Package 3 (1680ft - 4500ft)

Al_2O_3 was primarily controlled by kaolinite with values of 2% and 6.26%. K_2O was mainly controlled by either illite/muscovite and/or jarosite with value of 0.19% and 0.86%, respectively. Na_2O could have been controlled by Na containing minerals including plagioclase. Fe_2O_3 was mainly controlled by pyrite and jarosite, but with little contribution from illite/muscovite and/or chlorite (Table 7).

3.4 Integration of chemostratigraphy with already existing biostratigraphic data

The shale of the two wells, i.e. #3 and Sahaiawei-1 wells, each had its own distinctive geochemical fingerprint. This was so because the geochemistry varies distinctly between lithologies and depth. Generally, biostratigraphic units in hydrocarbon basins are defined using the traditional methods of zonation (palynological zones, foraminiferal zones and nannofossil zones). These methods of zonation do not always produce the required stratigraphic resolution for geologic modelling, particularly when dealing with sequences that are barren of fossils and successions that contain monotonous shale deposits [1, 5, 10, 36]. Consequently, there is need for a multidisciplinary approach that will add further resolution to the internal stratigraphic architecture of these depobelts; an approach that can aid in the characterization and correlation of the hydrocarbon reserves in the area.

Chemostratigraphic characterization and correlation was carried out across both wells based on the steps of interpretative methodology [1, 4, 6-8, 10]. This correlation was based strictly on chemical signature and not chronostratigraphic markers. The package 1 of #3 well was constrained to the P540, P560, P540 and part of P620-P630 Zones of Evamy *et al*. [14]; and the Lower N2-N4 Zone of Blow [26, 27]. The two sequence boundaries and maximum flooding surfaces were confined to package 1 (Figure 8). The geochemical boundary 1(GB 1) was constrained to P620-P630 Zone. The package 2 was constrained to part of the P620-P630 and P650-P670, and N4-N5 Zones. Packages 3 and 4; and geochemical boundaries 2 and 3 could not be tied to any palynological zones, and they may be within zones that are constrained to the other palynological zones of Evamy *et al*. [14].

On the other hand, package 1 of the Sahaiawei-1 well was constrained to the P200, P330-P430, P450 and part of the P470 Zones of Evamy *et al*. [14]; and the M18, P1-P2, P3-P4, P5/P6-P7, P7-P13 Zones of Blow [26, 27]. The sequence boundary and three maximum flooding surfaces were constrained to the package 1 (Figure 9). The geochemical boundary (GB) 1 was constrained to the P470 Zone. Package 3 was constrained to part of the P470 and P480 Zones of Evamy *et al*. [14].

Table 6. Bulk XRD percentage for Sahaiawei-1 well

Depth (ft)	Clays minerals (%)				Carbonates (%)		Other minerals (%)									Total (%)
	Kao.	Ill./ Mu.	Chl.	Sep.	Car.	Dol.	Qtz.	Pyr.	Ana.	Gyp.	Pla.	Mic.	Jar.	Bar.	Flu.	
3060 (Pk. 3)	2	0.19	0.03	0	0	0	96	0	0	0.92	0	0	0.86	0	0	100
4500 (Pk. 3)	6.26	0	0	0.48	0	0	91.5	0.16	0.05	1.48	0	0	0	0	0.04	99.97
5160 (Pk. 1)	39.8	1	0.28	2.87	0.17	0	41.3	0.56	0.55	4.9	2.77	5.04	0.61	0	0	99.85
6240 (Pk. 1)	23.7	1.48	0	2.08	31.20	3.17	29.3	1.99	0.34	5.68	0	0	0	0.15	0.14	99.23
7440 (Pk. 1)	25.34	2.3	1.68	4.79	2.71	14.20	41.1	1.54	0.61	3.55	0	1.48	0	0.67	0	99.97
8700 (Pk. 1)	29.2	3.94	1.71	10.1	4.17	2.40	23.9	0.77	0.79	0.28	0.13	0	0	22.5	0	99.89
9300 (Pk. 1)	37.83	2.91	2.68	4.38	1	2.59	38.4	1.52	1.13	4.73	1.78	0.96	0	0.08	0	99.99
10620 (Pk. 1)	7.22	1.96	0.34	1.82	22.73	8.52	22.6	1	0.32	0.74	6.97	0	0	7.34	18.2	99.76

Table 7. The Mineralogical control on key elements in Sahaiawei-1 Well

Packages	Key elements			
	Al_2O_3	K_2O	Na_2O	Fe_2O_3
Package 3 (1680ft-4500ft)	kaolinite	Jarosite, Illite/muscovite	Plagioclase?	Jarosite, Illite/muscovite, Pyrite, Chlorite,
Package 1 (4860ft-10620ft)	Kaolinite	Illite/muscovite, Microcline	Plagioclase	Illite/muscovite, Chlorite, Pyrite

Some elements function as proxies for environmental conditions during deposition [36]. The primary elemental proxies this work focuses on were Al_2O_3, K_2O, Na_2O, Fe_2O_3 and TiO_2. Aluminum oxide (Al_2O_3) and potassium oxide (K_2O) are associated with clay minerals and alkali feldspar (K- feldspar), respectively [35, 37]; while TiO_2 is associated with continental derived sediments [38, 39]. Clay minerals can travel to more distant regions of the basin; whereas potassium oxide (K_2O) grain will behave hydrodynamically like sand and silt size grains. Hence, increase in Al_2O_3 and K_2O with a decline in TiO_2, can be interpreted that the depositional environment is becoming more distal with regard to the source of sedimentation [35, 37]. In both wells, the highest concentration of clay proxies (Al_2O_3 and K_2O) occurred in package 1 with a low percentage of TiO_2 (Tables 2 and 3), which can be seen as evidence of the environment of depositional was becoming more distal with regard to the source of sedimentation. During the Early to Late Oligocene and Late Maastrichtian, the environmental of deposition was more of a marine environment. The concentration of Al_2O_3 and K_2O decreased markedly across packages 2, 3 and 4; while TiO_2 increased and fluctuated slightly (Tables 2 and 3), which can be interpreted in terms of environment of deposition during the Paleocene to Early Eocene and Oligocene becoming transitional to continental environment.

The mineralogical control on the key elements identified for both wells were clay minerals (kaolinite, illite/muscovite, and chlorite), plagioclase, microcline, jarosite and pyrite. Kaolinite had more control than other minerals on the distribution of the key elements in the wells. High percentages of kaolinite to illite ratio implied that as the degree of hydrolytic weathering was high, the sediments were more kaolinitic [3]. The high percentage of kaolinite over illite (Tables 4 and 6) from packages 1, 2, 3 and 4 across the two wells implied that the degree of hydrolytic weathering was high. The sediments were more kaolinitic. The kaolinites were formed in hot humid climates as a result of leaching and transporting of Na+, K+ and Ca+ in solution during weathering of feldspathic minerals [40].

Integrating chemostratigraphy with biostratigraphy showed that the geochemical control across the wells were lateral. The #3 and Sahaiawei-1 wells were from different depobelts and they were not of the same time equivalent age. Thus, integrating chemostratigraphy with biostratigraphic information from both wells revealed that the geochemical control across both wells was lateral despite them being of different ages.

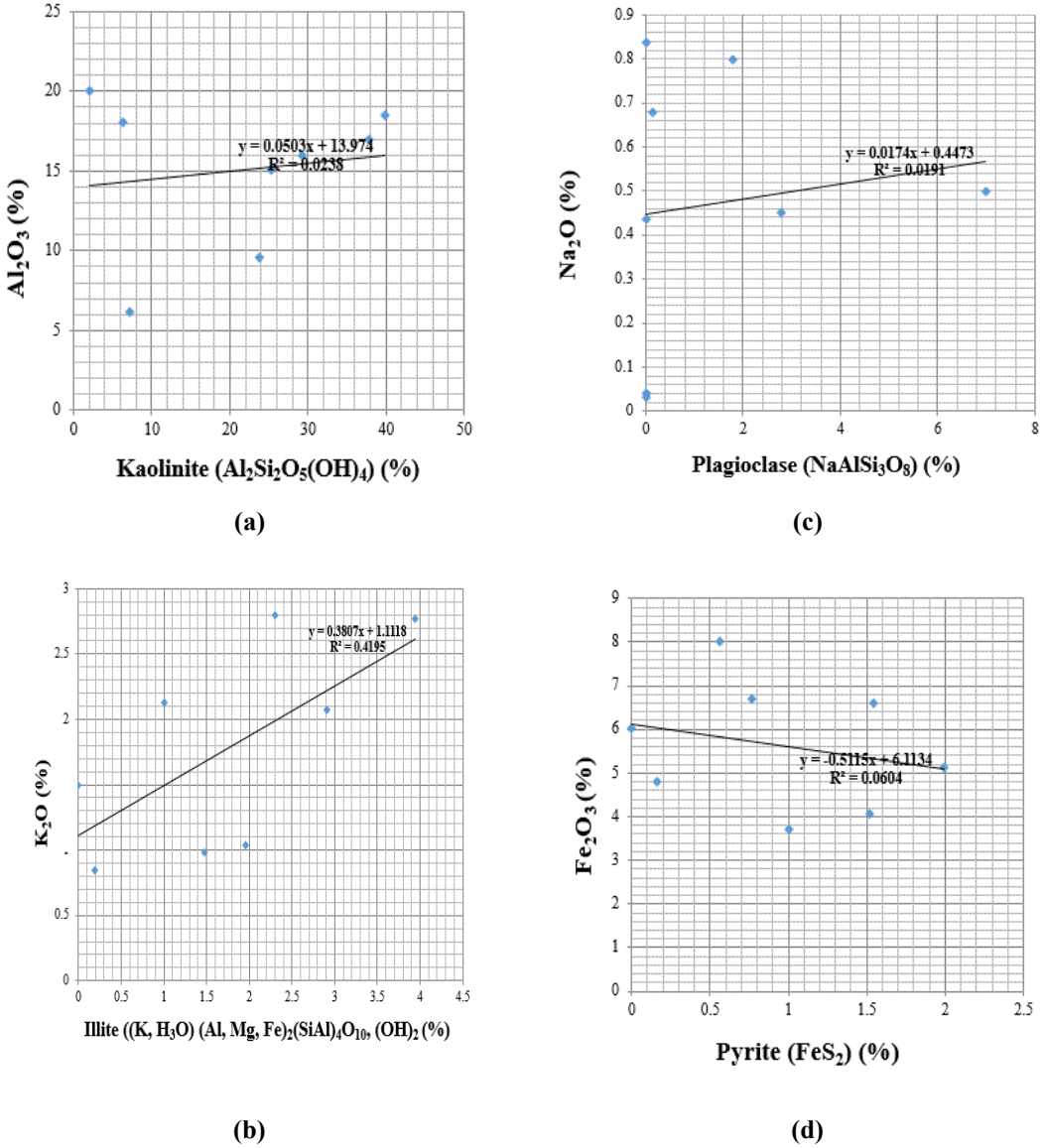

Figure 7. Binary diagram of kaolinite against Al_2O_3 for Sahaiawei-1 Well (a); illite against K_2O for Sahaiawei-1 Well (b); plagioclase against Na_2O for Sahaiawei-1 Well (c) and Pyrite against Fe_2O_3 for Sahaiawei-1 Well (d)

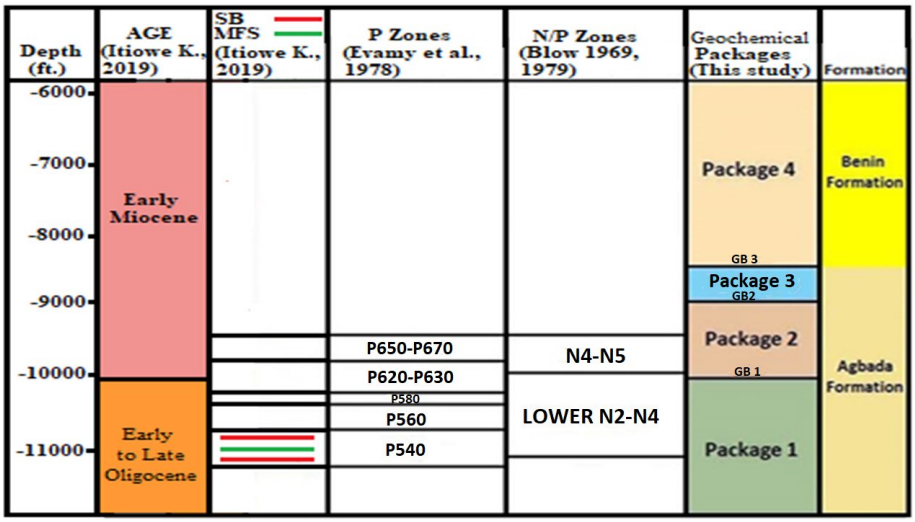

Figure 8. Integration of chemostratigraphy with biostratigraphic data for #3 well

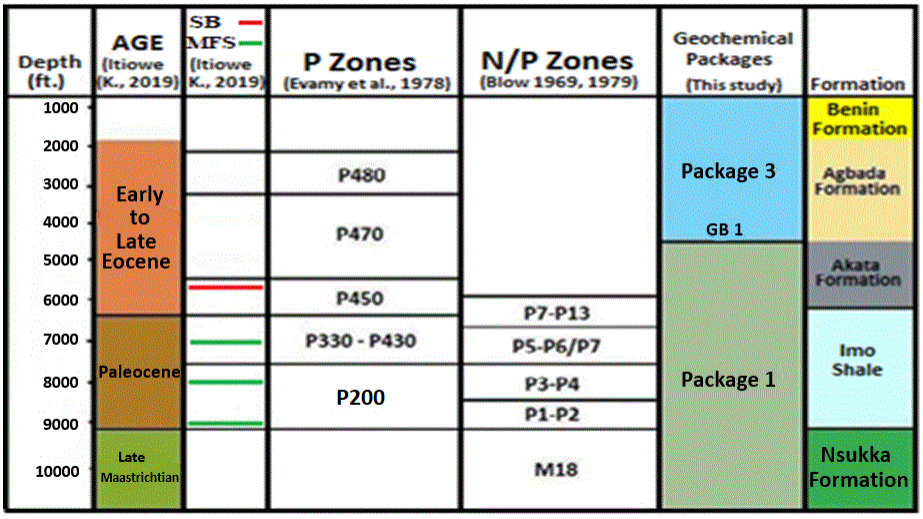

Figure 9. Integration of chemostratigraphy with biostratigraphic data for Sahaiawei-1 well

4. Conclusions

This study demonstrated the integration of chemostratigraphy to already existing biostratigraphic data. A successful chemostratigraphic characterization and correlation across both wells was achieved in this study. This correlation was based strictly on chemical signatures and not on chronostratigraphic markers. Four geochemical packages and three geochemical boundaries were identified for #3 well, while two geochemical packages and one geochemical boundary was identified for Sahaiawei-1 well. The mineralogical control on the key elements identified for both wells were clay minerals (kaolinite, illite/muscovite, and chlorite), plagioclase, microcline, jarosite

and pyrite, with kaolinite having more control in the differentiation of the key elements than other minerals.

The key elements used for chemostratigraphic characterization and correlation were consistent in both wells and were used to define some informal geochemical markers and events (geochemical packages and boundaries) in the Greater Ughelli and Northern Delta depobelts. These geochemical markers and events will improve the inorganic geochemistry and chronostratigraphic chart of the Niger Delta. Furthermore, this study introduced a multidisciplinary approach to provide detailed stratigraphic architecture as well as identification of some regional geochemical markers. Our work should, in future, facilitate easy seismic interpretation and identification of the Niger Delta petroleum elements at play. Finally, this study demonstrated that chemostratigraphy had the ability to complement the existing biostratigraphic schemes, thereby providing a means to unify stratigraphic schemes within any petroleum basin.

5. Acknowledgement

The authors are grateful to NPDC for provision of ditch cutting samples, the staff of the Nigeria Geological Survey Agency (NGSA), Kaduna for the technical assistance during the use of their XRF machine, the staff of XRD Analytical and Consulting Company, South Africa, for the XRD analysis. Also, we thank Ross McCabe of Chemostrat Ltd for his assistance during the chemostratigraphic correlation and interpretation.

References

[1] Pearce, T.J., Wray, D.S., Ratcliffe, K.T., Wright, D.K. and Moscarello, A., 2005. Chemostratigraphy of the upper carboniferous Schooner formation, southern North Sea. In: J.D. Collinson, D.J. Evans, D.W. Holliday and N.S. Jones, eds. *Carboniferous Hydrocarbon Geology: the Southern North Sea and Surrounding Onshore Areas*. London: Yorkshire Geological Society, pp. 147-164.

[2] Ratcliffe, K.T., Morton, A., Ritcey, D. and Evenchick, C.E., 2007. Whole rock geochemistry and heavy mineral analysis as exploration tools in the Bowser and Sustut Basins, British Colombia, Canada. *Journal of Canadian Petroleum Geology*, 55, 320-337, DOI: 10.2113/gscpgbull.55.4.320.

[3] Ratcliffe, K.T., Wright, A.M., Montgomery, P., Palfrey, A., Vonk, A., Vermeulen, J. and Barrett, M., 2010. Application of chemostratigraphy to the Mungaroo formation, the Gorgon field, offshore Northwest Australia. *APPEA Journal*, 50, 371-385, DOI: 10.1071/AJ09022.

[4] Wright, A.M., Ratcliffe, K., Bhattacharya, J., Zhu, Y. and Wray, D.S., 2010. *The Application of Chemostratigraphy to Fluvial-Deltaic Sequences: Example from the Ferron Sandstone Member, South-Central Utah*. [online] Available at: https://www.searchanddiscovery.com/documents/2010/40498wright/ndx_wright.pdf.

[5] Ratcliffe, K.T., Wright, A.M., Hallsworth, C., Morton, A., Zaitlin, B.A., Potocki, D. and Wray, D.S., 2004. An example of alternative correlation techniques in a low accommodation setting, non-marine hydrocarbon system: the (Lower Cretaceous) Mannville Basal Quartz succession of southern Alberta. *American Association of Petroleum Geologists Bulletin*, 88, 1419-1432, DOI: 10.1306/05100402035.

[6] Craigie, N.W., Pierre, B. and Ahmed, K., 2016. Chemostratigraphy and biostratigraphy of Devonian, Carboniferus and Permian sediments encountered in the eastern Saudi Arabia: An

integrated approach to reservoir correlation. *Marine and Petroleum Geology*, 72, 156-178. DOI: 10.1016%2Fj.marpetgeo.2016.01.018.

[7] Craigie, W.N., 2021. Chemostratigraphy and its application in integrated reservoir correlation. In: E. Onajite, ed. *Applied Techniques to Integrated Oil and Gas Reservoir Characterization.* Amsterdam: Elservier, pp. 73-115.

[8] Craigie, W.N., 2018. *Principles of Elemental Chemostratigraphy*. Cham: Springer.

[9] Craigie, W.N., 2016. Chemostratigraphy of the Silurian Qusaiba Member, Eastern Saudi Arabia. *Journal of African Earth Sciences,* 113, 12-34, DOI: 10.1016/j.jafrearsci.2015.10.007.

[10] Prundeanu, I.M., Chelariu, C. and Perez, D.R.C., 2021. Elemental geochemistry of the upper cretaceous reservoir and surrounding formations applied in geosteering of horizontal wells, Lebăda Field – Western Black Sea. *Oil and Gas Science and Technology- Revue d'IFP Energies Nouvelles*, 76, DOI: 10.2516/ogst/2020083.

[11] Mejia, C., Nardi, G. and Iain, D., 2018. Integration of LWD and geochemistry from cuttings measurements for well placement based on real time diagenesis characterization. *Offshore Technology Conference*, Houston, Texas, April 30-May 3, 2018, DOI: 10.4043/29040-MS.

[12] Fačevicova, K., Bábek, O., Hron, K. and Kumpan, T., 2016. Element chemostratigraphy of the Devonian/Carboniferous boundary – A compositional approach. *Applied Geochemistry*, 75, 211-221, DOI: 10.1016/j.apgeochem.2016.10.002.

[13] Weber, K.J. and Daukoru, E.M., 1975. Petroleum geology of the Niger Delta. *Proceedings of the 9th World Petroleum Congress*, Tokyo, Japan, May 11-16, 1975, pp. 210-221.

[14] Evamy, B.D., Haremboure, J., Kamerling, P., Knaap, W.A., Molloy, F.A. and Rowlands, P.H., 1978. Hydrocarbon habitat of Tertiary Niger Delta. *American Association of Petroleum Geologists Bulletin,* 62, 277- 298.

[15] Frankl, E.J. and Cordry, E.A., 1967. The Niger Delta oil province: recent developments onshore and offshore. *Proceedings of 7th World Petroleum Congress*, Mexico City, Mexico, April 2-9, 1967, pp. 125-209.

[16] Short, K.C. and Stauble, A.J., 1967. Outline geology of Niger Delta. *American Association of Petroleum Geologists Bulletin*, 51, 761-779.

[17] Avbovbo, A.A., 1978. Tertiary lithostratigraphy of Niger Delta. *American Association of Petroleum Geologists Bulletin*, 62, 295-300.

[18] Ejedawe, J.E., Coker, S.J.L., Lambert-Alkhionbare, D.O., Aloof, K.B. and Adult, F.O., 1984. Evolution of oil generation window and oil and gas occurrence in Tertiary Niger Delta Basin. *American Association of Petroleum Geologists Bulletin*, 68, 1744-1751.

[19] Nwachukwu, J.L. and Chukwura, C., 1986. Organic matter of Agbada formation, Niger Delta, Nigeria. *American Association of Petroleum Geologists Bulletin*, 70, 48-55.

[20] Haack, R.C., Sunderaman, P., Diedjomahor, J.O., Xiao, H., Gant, N.J., May, E.D. and Kelsch, K., 2000. Niger delta petroleum system, Nigeria. In: M.R. Mello and B.J Kat, eds. *Petroleum Systems of South Atlantic Margins*. Tulsa: America Association of Petroleum Geologist, pp. 213-231.

[21] Reijers, T.J.A., 2011. Stratigraphy and sedimentology of the Niger Delta. *Geologos,* 17(3), 133-162, DOI: 10.2478/v10118-011-0008-3.

[22] Cohen, H.A. and McClay, K., 1996. Sedimentation and shale tectonics of the North-Western Niger Delta front. *Marine and Petroleum Geology*, 13(3), 313-328, DOI: 10.1016/0264-8172(95)00067-4.

[23] Whiteman, A.J., 1982. *Nigeria: Its Petroleum Geology, Resources and Potential*. Vol. 1&2. Edinburgh: Graham & Trotman.

[24] Itiowe, K. and Lucas, F.A., 2020. Palynological zonation and paleoclimatic condition of the sediments penetrated by ash-3 well in the Greater Ughelli Depobelt, Niger Delta Basin. *International Journal of Pure and Applied Sciences*, 19(1), 37-48.

[25] Itiowe, K. and Lucas, F.A., 2020. Foraminiferal biostratigraphy and paleoenvironmental study of the sediments penetrated within the interval of 6030ft. to 11115ft. of ash-3 well in the greater Ughelli Depobelt, Niger Delta Basin. *International Journal of Pure and Applied Sciences*, 19(1),130-150.

[26] Blow, W.H., 1969. Late miocene to recent planktonic foraminifera biostratigraphy. In P. Brönnimann and H.H. Renz, eds. *Proceedings of the First International Conference on Planktonic Microfossils*. Vol 1. Leiden: E.J. Brill, pp. 199-422.

[27] Blow, W.H., 1979. *The Cenozoic Globigerinida*. Vol. 3. Leiden: E.J. Brill.

[28] Kiamuke, I., Adebayo, L.F. and Rorome, O., 2021. Palynological and paleoclimatic conditions of the sediments penetrated by Sahaiawei-1 well in the Northern Delta Depobelt, Niger Delta Basin. *Journal of Mining and Geology*, 5(1), 47-54.

[29] Itiowe, K., Lucas, F.A. and Olise, C.O., 2020. Foraminiferal biostratigraphy and paleoenvironmental analysis of the sediments penetrated by Sahaiawei-1 well in the Northern Delta Depobelt, Niger Delta Basin. *Global Journal of Geological Series*, 18, 119-126, DOI: 10.4314/gjgs.v18i1.10.

[30] Itiowe, K., 2019. *Lithofacies, Biostratigraphy and Chemostratigraphy of Two Wells in the Niger Delta Basin*. Ph.D. Thesis, University of Benin, Nigeria.

[31] Lemiere, B., 2018. A review of pXRF (field portable x-ray fluorescence) applications for applied geochemistry. *Journal of Geochemical Exploration,* 188, 350-363, DOI: 10.1016/j.gexplo.2018.02.006.

[32] David, W.I.F., Shankland, K., McCusker, L.B. and Baerlocher, C., 2002. *Structure Determination from Powder Diffraction Data*. Oxford: Oxford University Press.

[33] Will, G., 2006. *Powder Diffraction: The Rietveld Method and the Two Stage Method to Determine and Refine Crystal Structures from Powder Diffraction Data*. Berlin: Springer-Verlog.

[34] Moore, D.M. and Reynolds R.C., Jr., 1989. *X-ray Diffraction and the Identification and Analysis of Clay Minerals*. New York: Oxford University Press.

[35] Pearce, T.J., Besly, B.M., Wray, D.S. and Wright, D.K., 1999. Chemostratigraphy: a method to improve interwell correlation in barren sequences – a case study using onshore Duckmantian/Stephanian sequences (West Midlands, U.K.). *Sedimentary Geology*, 124, 197-220, DOI: 10.1016/S0037-0738(98)00128-6.

[36] Ikhane P.R., Akintola A.I., Bankole S.I., Ajibade O.M. and Edward O.O, 2014. Chemostratigraphic characterization of siliciclastic rocks in parts of the Eastern Dahomey Basin, Southwestern Nigeria. *Journal of Geography and Geology*, 6, 88-108, DOI: 10.5539/jgg.v6n4p88.

[37] Tribovillard, N., Algeo, T.J., Lyons, T. and Riboulleau, A., 2006. Trace metals as paleoredox and paleoproductivity proxies: an update. *Chemical Geology*, 232, 12-32, DOI: 10.1016/j.chemgeo.2006.02.012.

[38] Bhatia, M.R. and Crook, K.A.W., 1986. Trace element characteristics of graywackes and tectonic setting discrimination of sedimentary basins. *Contributions to Mineralogy and Petrology*, 92, 181-193, DOI: 10.1007/BF00375292.

[39] Sageman, B.B. and Lyons, T.W., 2004. Geochemistry of fine-grained sediments and sedimentary rocks. In: F.T. Mackenzie, ed. *Treatise on Geochemistry*. Vol. 7. Amsterdam: Elsevier, pp.115-158.

[40] Zhang, C., Guo, Z., Deng, C., Ji, X., Wu, H, Paterson, G.A., Chang, L., Li, Q., Wu, B. and Zhu, R., 2016. Clay mineralogy indicates a mildly warm and humid living environment for the Miocene hominoid from the Zhaotong Basin, Yunnan, China. *Scientific Reports,* 6, DOI: 10.1038/srep20012.